Nano Res. 2012, 5(1): 49–61
DOI 10.1007/s12274-011-0184-z
Research Article

ISSN 1998-0124
CN 11-5974/O4

Size-Tunable Nanoparticles Composed of Dextran-*b*-poly(*D*,*L*-lactide) for Drug Delivery Applications

Mohit S. Verma[1,§], Shengyan Liu[1,§], Yih Y. Chen[1], Ameena Meerasa[1], and Frank X. Gu[1,2] (✉)

[1] Department of Chemical Engineering, University of Waterloo, Waterloo N2L 3G1, Canada
[2] Waterloo Institute for Nanotechnology, University of Waterloo, Waterloo N2L 3G1, Canada
[§] These authors contributed equally to this work

Received: 5 September 2011 / Revised: 19 October 2011 / Accepted: 28 October 2011

ABSTRACT

Nanoparticles (NPs) formulated using self-assembly of block copolymers have attracted significant attention as nano-scaled drug delivery vehicles. Here we report the development of a biodegradable NP using self-assembly of a linear amphiphilic block copolymer, Dex-*b*-PLA, composed of poly(*D*,*L*-lactide), and dextran. The size of the NPs can be precisely tuned between 15 and 70 nm by altering the molecular weight (M_W) of the two polymer chains. Using doxorubicin as a model drug, we demonstrated that the NPs can carry up to 21% (*w*/*w*) of the drug payload. The release profile of doxorubicin from NPs showed sustained release for over 6 days. Using a rat model, we explored the pharmacokinetics profiles of Dex-*b*-PLA NPs, and showed proof-of-concept that long circulation lifetime of the NPs can be achieved by tuning the M_W of Dex-*b*-PLA block copolymer. While the terminal half-life of Dex-*b*-PLA NPs (29.8 h) was similar to that observed in poly(ethylene glycol)-coated (PEG-coated) NPs (27.0 h), 90% of the injected Dex-*b*-PLA NPs were retained in the blood circulation for 38.3 h after injection, almost eight times longer than the PEG-coated NPs. The area under curve (AUC) of Dex-*b*-PLA NPs was almost four times higher than PEG-based NPs. The biodistribution study showed lower accumulation of Dex-*b*-PLA NPs in the spleen with 19.5% initial dose per gram tissue (IDGT) after 24 h compared to PEG-coated poly(lactide-*co*-glycolide) (PLGA) NPs (29.8% IDGT). These studies show that Dex-*b*-PLA block copolymer is a promising new biomaterial for making controlled nanoparticles as drug delivery vehicles.

KEYWORDS

Dextran, nanoparticles, biodistribution, pharmacokinetics, controlled drug delivery, *in vivo*

1. Introduction

Nanomedicine—the fusion of nanotechnology and medicine—is among the most promising approaches to address challenges associated with conventional drug delivery methods [1]. In the past decade, drug delivery systems constructed from polymeric nanoparticles (NPs) have been the cornerstone of progress in the field of nanomedicine [2–4]. Various types of polymeric materials composed of poly(*D*,*L*-lactide) (PLA), poly(glycolide) (PGA), poly(lactide-*co*-glycolide) (PLGA), and poly(ε-caprolactone) (PCL), have been studied extensively for NP drug delivery applications [5, 6]. To date, masking the NP surface with poly(ethylene glycol) (PEG) has been the most effective strategy to improve the stabilities of NP

Address correspondence to frank.gu@uwaterloo.ca

drug delivery systems *in vitro* and *in vivo* [7–13]. PEGylated NPs with sizes under 70 nm in diameter have the potential of bypassing the reticuloendothelial system (RES), which leads to prolonged circulation half-life of the particles [14]. Particles with size smaller than 100 nm preferentially accumulate at the tumor site by the enhanced permeation and retention (EPR) effect and also evade the organs of the RES [15]. Once the NPs reach the intended tumor site, the rate of NP uptake by the tumor cells is largely influenced by the particle size. It has been demonstrated that rapid cellular uptake of NPs can be achieved when the particle size falls below 50 nm [16]. PLGA–PEG is the most widely used polymer for making biodegradable drug delivery systems. However, the self-assembly of PLGA–PEG block copolymers generally yields NPs of sizes greater than 150 nm [17]. Although smaller particles can be synthesized, they suffer from low drug encapsulation and rapid drug release [17]. An emerging strategy for making PLGA–PEG NPs under 100 nm is by rapidly mixing the block copolymers in a microfluidics device [17].

Here, we reported the synthesis of a linear block copolymer using PLA and dextran (Dex-*b*-PLA), and demonstrated that NPs composed of Dex-*b*-PLA can self-assemble into core–shell structured NPs with sizes less than 40 nm without using any flow-focusing devices. We further showed that the size of Dex-*b*-PLA NPs can be precisely fine-tuned between 15–70 nm by altering the molecular weight (M_W) of the component blocks. Dextran, a natural polysaccharide composed of 1→6 linked *α*-*D*-glucopyranosyl units, was selected as a model hydrophilic block because of its high hydrophilicity and biocompatibility. Studies have shown that dextran-coated NPs showed superior colloidal stability compared to those coated with PEG chains [18]. Dextran and PLA have been explored together in the synthesis of PLA–*graft*–Dex [19]. However, dextran-grafted copolymers have a major limitation because grafting density (i.e., the number of PLA units per dextran backbone unit) is difficult to control, and the grafting is limited only to low M_W PLA as opposed to high M_W PLA. In this study, linear block copolymers composed of dextran and PLA were synthesized, and the size and morphologies of the NPs formed from Dex-*b*-PLA were systematically controlled by varying their composition. The drug encapsulation efficiencies of the NPs and their release kinetics were also evaluated using doxorubicin as a model hydrophobic anti-cancer drug. The hemolytic activity of the NPs was tested to profile the biocompatibility of the NPs in systemic circulation, and the blood circulation half-life and biodistribution of the NPs in rats were assessed.

2. Experimental

2.1 Materials

Acid-terminated poly(*D*,*L*-lactide) (PLA, M_W ~10, 20, and 50 kDa) and PLGA–PEG (PLGA M_W ~40 kDa, PEG M_W ~6 kDa) were purchased from Lakeshore Biomaterials (Birmingham, AL, USA). PLA was purified by dissolving in dimethyl sulfoxide (DMSO) and precipitating in methanol to remove residual monomers. Dextran (Dex, relative molecular mass (M_r) ~1.5, 6, and 10 kDa), hydrochloric acid (HCl), triethylamine (TEA), *N*-(3-dimethylaminopropyl)-*N*-ethylcarbodiimide (EDC), and sodium cyanoborohydride ($NaCNBH_3$) were purchased from Sigma Aldrich (Oakville, ON, Canada), and used without further purification. *N*-Hydroxysulfosuccinimide (Sulfo-NHS) and *N*-Boc-ethylenediamine were purchased from CNH Technologies (Massachusetts, USA). Doxorubicin–HCl (M_W = 580 Da, Intatrade GmBH, Bitterfield, Germany) was deprotonated by adding TEA (2 mol equivalents) to an aqueous solution of doxorubicin–HCl, and the hydrophobic form of doxorubicin was extracted using dichloromethane (DCM) [20]. Borate buffer was prepared at a concentration of 0.05 mol/L with pH of 8.2 by mixing boric acid and sodium hydroxide. Whole sheep blood (in Alsevers solution) was purchased from Cedarlane (Burlington, ON, Canada). Veronal buffer solution (VBS, 5x) was purchased from Lonza Walkersville Inc (Walkersville, MD, USA). Tritium [^{3}H]-PLA-radiolabeled nanocrystals were purchased from PerkinElmer (Boston, MA, USA).

2.2 Synthesis of Dex-*b*-PLA

The synthesis of the linear block copolymer is divided into three stages: (1) reductive amination between dextran and *N*-Boc-ethylenediamine, (2) deprotection

of the Boc group, and (3) conjugation of the end modified dextran with PLA (Scheme 1). The first step of the synthesis involves reductive amination between the aldehyde on the reducing end of dextran and the amine group of *N*-Boc-ethylenediamine cross-linker. In a typical reaction, Dex6 (M_r ~6 kDa, 6 g, 1 mmol) was dissolved in 15 mL of borate buffer (0.05 mol/L, pH 8.2) with 4 g (2.5 mmol) of *N*-Boc-ethylenediamine. The reducing agent, $NaCNBH_3$ (1 g, 15 mmol), was added to the borate buffer solution and the mixture was stirred for 72 h in dark conditions at room temperature. The mixture was then washed in methanol to remove any unreacted molecules or catalysts. The end-modified dextran was dried overnight *in vacuo*. ^{1}H Nuclear Magnetic Resonance (^{1}H NMR) samples were prepared by dissolving the end-modified dextran in D_2O (30 mg/mL). The dried dextran was re-dissolved in deionized water (DI-H_2O). The deprotection of Boc group was performed first by adding HCl (~4 mol/L) for 1 h to cleave the amide bond between the Boc group and the protected amine moiety. Subsequently, TEA was added to increase the pH of the solution to 9 to deprotonate the $-NH_3^+$ end groups which were deprotected. The mixture was then washed twice using methanol and dried *in vacuo*. An NMR sample of the dried product was prepared in D_2O (30 mg/mL). The amine-terminated dextran and carboxyl-terminated PLA20 (M_W ~20 kDa, 6 g, 0.3 mmol) were dissolved in DMSO. The conjugation between the two polymers was facilitated by adding catalysts EDC (120 mg, 0.773 mmol) and Sulfo-NHS (300 mg, 1.38 mmol) and allowing the reaction to proceed for 4 h at room temperature. The resulting Dex-*b*-PLA was twice precipitated and purified using excess methanol. In order to remove free dextran, the mixture was dissolved in acetone (30 mL) to form a cloudy suspension. This was centrifuged at 4000 r/min for 10 min and the supernatant was

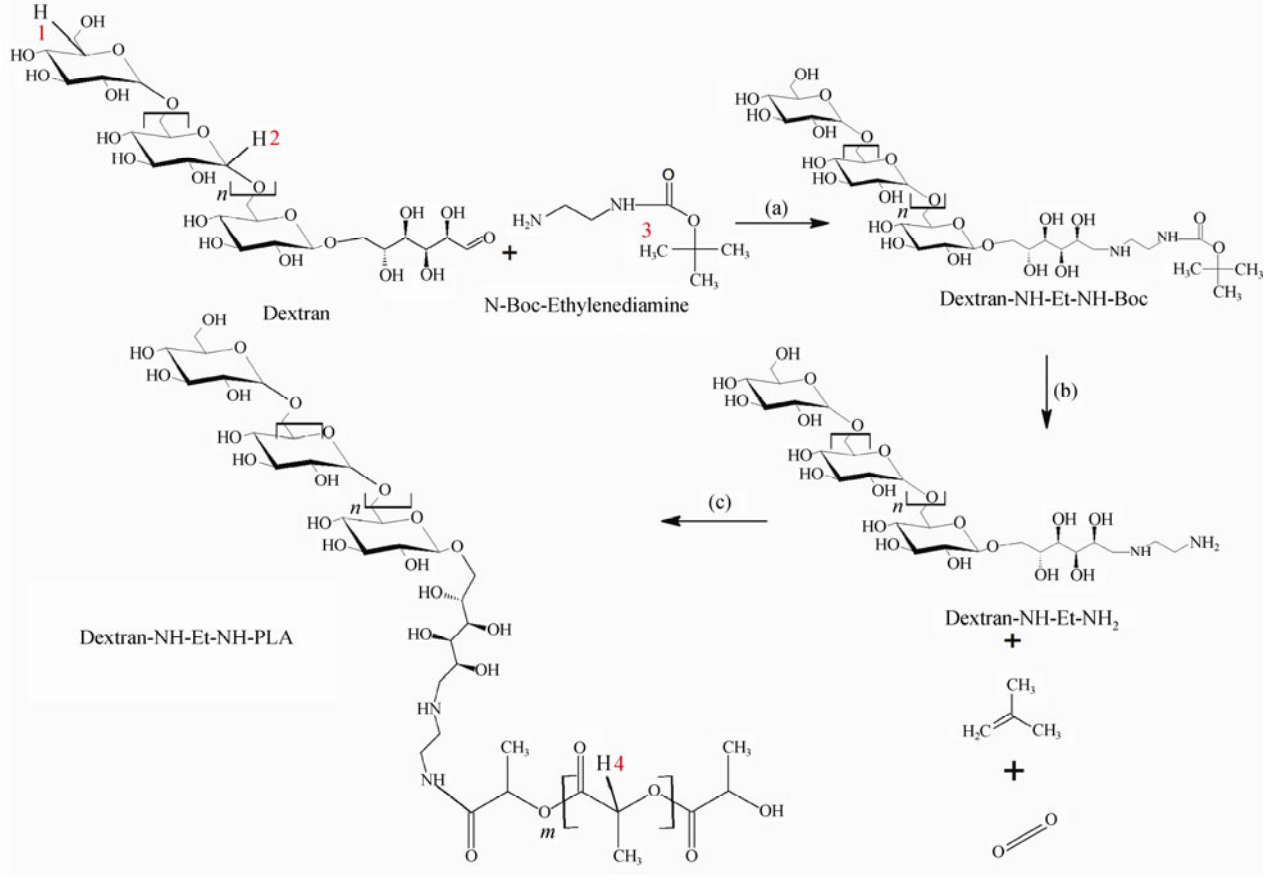

Scheme 1 Synthesis of Dex-*b*-PLA block copolymers. (a) Synthesis of dextran-NH-Et-NH-Boc. Conditions: $NaCNBH_3$ in borate buffer (pH 8.2) for 72 h at room temperature (RT) in the dark; (b) synthesis of dextran-NH-Et-NH_2. Conditions: HCl/TEA in deionized water for 1 h each at room temperature; (c) synthesis of dextran-NH-Et-NH-PLA. Conditions: EDC/Sulfo-NHS RT for 4 h

purged with air to remove the solvent and then dried overnight *in vacuo* to obtain the final copolymers. NMR samples were prepared at a concentration of 30 mg/mL in DMSO-d6 for proton NMR and 150 mg/mL in DMSO-d6 for carbon-13 NMR.

2.3 Characterization of Dex-*b*-PLA using nuclear magnetic resonance

The various stages of Dex-*b*-PLA synthesis were verified using ^{1}H NMR spectroscopy (Bruker 300 MHz). The final polymer conjugation was also verified using ^{13}C NMR spectroscopy (Bruker 300 MHz). Before any modification, dextran was dissolved in D_2O (30 mg/mL) and acid-terminated PLA was dissolved in $CDCl_3$ (5 mg/mL) for preparing NMR samples. As mentioned in the previous synthesis methods, the end products from the first two steps were dissolved in D_2O, whereas the final product, Dex-*b*-PLA, was dissolved in DMSO-d6 for the NMR analysis.

2.4 Dex-*b*-PLA NP formation by nanoprecipitation

The Dex-*b*-PLA NPs were prepared using a nanoprecipitation method: 1 mL of Dex-*b*-PLA in DMSO (10 mg/mL) was added in a drop-wise manner to 10 mL of DI-H_2O under constant stirring in order to form NPs. This was stirred for 30 min and then dynamic light scattering (DLS) samples were prepared by extracting 3 mL samples into polystyrene cuvettes. The sizes of the NPs were analyzed using a 90Plus Particle Size Analyzer (Brookhaven, λ = 659 nm at 90°). The volume-averaged multimode size distribution (MSD) mean diameters were reported.

2.5 Transmission electron microscopy

The particle size and the morphology of the Dex-*b*-PLA NPs were further verified using transmission electron microscopy (TEM, Philips CM10) with an accelerating voltage of 60 kV and a lanthanum hexaboride filament (LaB6). 300 Mesh Formvar coated copper grids (Canemco and Marivac) were used for this experiment. The NP suspension in water was prepared using the nanoprecipitation method as mentioned above. A drop of the NP suspension was placed onto the grid, and the grid was briefly stained with aqueous phosphotungstic acid solution. The copper grid with the NP suspension was dried under ambient environment overnight before imaging under TEM.

2.6 Encapsulation of doxorubicin in Dex-*b*-PLA NPs via nanoprecipitation

The encapsulation of doxorubicin in the Dex-*b*-PLA NPs was accomplished using a nanoprecipitation method. Dex-*b*-PLA and doxorubicin were both dissolved in DMSO (Dex-*b*-PLA concentration of 7 mg/mL, with varying drug concentrations). 1 mL of the DMSO solution was added drop-wise into 10 mL of water under stirring and stirring was then continued for an additional 30 min. The NPs in water were filtered through a syringe filter (pore size = 200 nm) to remove the drug aggregates and subsequently filtered through Amicon filtration tubes (molecular weight cut-off (MWCO) = 10 kDa, Millipore) to further remove any remaining free drugs in the suspension. The filtered NPs containing encapsulated doxorubicin were re-suspended and diluted in DMSO. The drug loading (wt.%) in the polymer matrix was calculated by measuring the concentration of the doxorubicin in the mixture by obtaining the absorbance of the solution at 480 nm using an Epoch Multi-Volume Spectrophotometer System (Biotek). The measurements were obtained in triplicate (n = 3, mean ± S.D). The absorbance measured by the same procedure using the polymers without the drugs was used as the baseline. The absorbance was correlated with the concentration of the doxorubicin in DMSO by using the standard calibration curve. The same procedure was used for PLGA–PEG to encapsulate doxorubicin for comparative analysis. The encapsulation efficiency (%) and drug loading (wt.%) were calculated using the two equations Eq. (1) and Eq. (2)

$$\text{Encapsulation efficiency (\%)} = \frac{\text{Mass of drug encapsulated}}{\text{Mass of initial drug feed}} \times 100\% \quad (1)$$

$$\text{Drug loading (wt.\%)} = \frac{\text{Mass of drug encapsulated}}{\text{Mass of the nanoparticle}} \times 100\% \quad (2)$$

2.7 *In vitro* release of doxorubicin from Dex-*b*-PLA NPs

Using the procedure described in the previous section,

drug-encapsulated NPs were prepared and filtered to remove non-encapsulated drug aggregates. A purified sample of NP–drug suspension was collected to measure the maximum absorbance and this was used as the 100% release point. Subsequently, the NP–drug suspension was injected into a Slide-A-Lyzer Dialysis cassette (MWCO = 20 kDa, Fisher Scientific) and dialyzed against 200 mL of phosphate buffered saline (PBS, pH 7.4) at 37 ˚C under mild stirring. At predetermined time intervals, 1 mL of the release medium was extracted and the same volume of fresh new PBS was added to the release medium. The extracted release medium was used to perform ultraviolet–visible (UV–Vis) absorption measurements at 480 nm in triplicate (n = 3, mean ± standard deviation (S.D.)). The release medium was replaced several times to maintain the concentration of doxorubicin in the medium below 3 μg/mL and to stay below the solubility limit of the doxorubicin in PBS. Replacing the medium was also expected to prevent the adhesion of released doxorubicin to the glass walls of the beaker or the magnetic stir bar. The release of doxorubicin from PLGA–PEG was also obtained by an identical procedure for comparative analysis. Free doxorubicin—without any polymer—release was also observed using the same procedure and all three release profiles from the NPs were normalized using the free doxorubicin release data along with encapsulation efficiency data. This normalization resulted in a release curve for encapsulated doxorubicin. All experiments were performed in a dark environment, and the beakers were sealed with Parafilm to prevent evaporation of PBS.

2.8 Hemolysis assay

Dex-*b*-PLA NPs were purified by using Amicon filtration tubes (MWCO = 10 kDa) and centrifugation at 4100 r/min for 30 min. A concentration range of NPs was obtained by this process. These NPs were then incubated at 37 ˚C for 1 h with 200 μL of sheep erythrocytes with a red blood cell concentration of 1×10^8 cells/mL to obtain a final volume of 1 mL per sample. The percentage hemolysis was calculated by measuring the absorbance at 415 nm using the absorbance at 500 nm as the baseline. The measurements were conducted in triplicate (mean ± S.D.). VBS solution was used as the negative control and DI-H_2O was used as the positive control. PLGA–PEG NPs were also prepared and tested in a similar manner for comparison.

2.9 Pharmacokinetics and biodistribution of Dex-*b*-PLA NPs

To ensure that all radioactivity administered to rats was associated with the particles, tritium [^{3}H]-PLA-radiolabeled nanocrystals were washed and purified in methanol prior to NP formation. Albino Wistar rats, body mass between 200 and 250 g, were fasted overnight but had free access to water. 200 μL of the NP formulations were prepared in NaCl 0.9% and injected intravenously into the tail vein at a dose of approximately 30 mg/kg. Blood (approximately 200 μL) was collected in heparinized microcentrifuge tubes by controlled bleeding of hind leg saphenous veins at the indicated time intervals. To characterize the biodistribution of NPs, rats were euthanized at 24 h after NP injections. Approximately 200 μL of blood was drawn by cardiac puncture from each mouse. Organs including heart, lungs, liver, spleen, and kidneys were harvested from each animal as described previously [21]. The ^{3}H content in the tissue and blood were assayed in a Wallac 1414 Liquid Scintillation Counter.

2.10 Statistical analysis

Statistical analysis was performed using the student t-test and statistical significance was assessed with $p < 0.01$.

3. Results and discussion

3.1 Synthesis and characterization of Dex-*b*-PLA

The synthesis of Dex-*b*-PLA block copolymers was analyzed using ^{1}H NMR spectroscopy. As shown in Fig. 1(a) Ⅰ, the multiplet at 4.86 ppm was assigned to the proton on carbon 1 of the dextran repeat units. The multiplet at 3.14 ppm was assigned to the proton on carbon 5 of the non-reducing end and the integration ratio between these two multiplets was used to confirm the M_W of dextran. The reductive amination reaction of dextran and *N*-Boc-ethylenediamine was confirmed by the presence of the peak at 1.3 ppm (Boc group) after removing unreacted free *N*-Boc-ethylenediamine (Fig. 1(a) Ⅱ). The subsequent deprotection of the Boc

group exposing the –NH_2 end-group on dextran was verified by the disappearance of the peak at 1.3 ppm (Fig. 1(a)Ⅲ). It was shown that the peak at 1.3 ppm was completely removed after the deprotection steps using HCl and TEA. After the conjugation of the –NH_2-terminated dextran with the –COOH-terminated PLA (Fig. 1(a)Ⅳ), the excess free dextran was removed by precipitating in acetone. The final product shows peaks corresponding to both dextran (multiplets at 4.86 ppm) and PLA (multiplets at 5.2 ppm) which confirms the conjugation of the two polymers (Fig. 1(a)Ⅴ). The linear end-to-end conjugation of PLA and dextran was also confirmed by ^{13}C NMR (Fig. 1(b)). The peak at 166.81 ppm is assigned to the carbon on

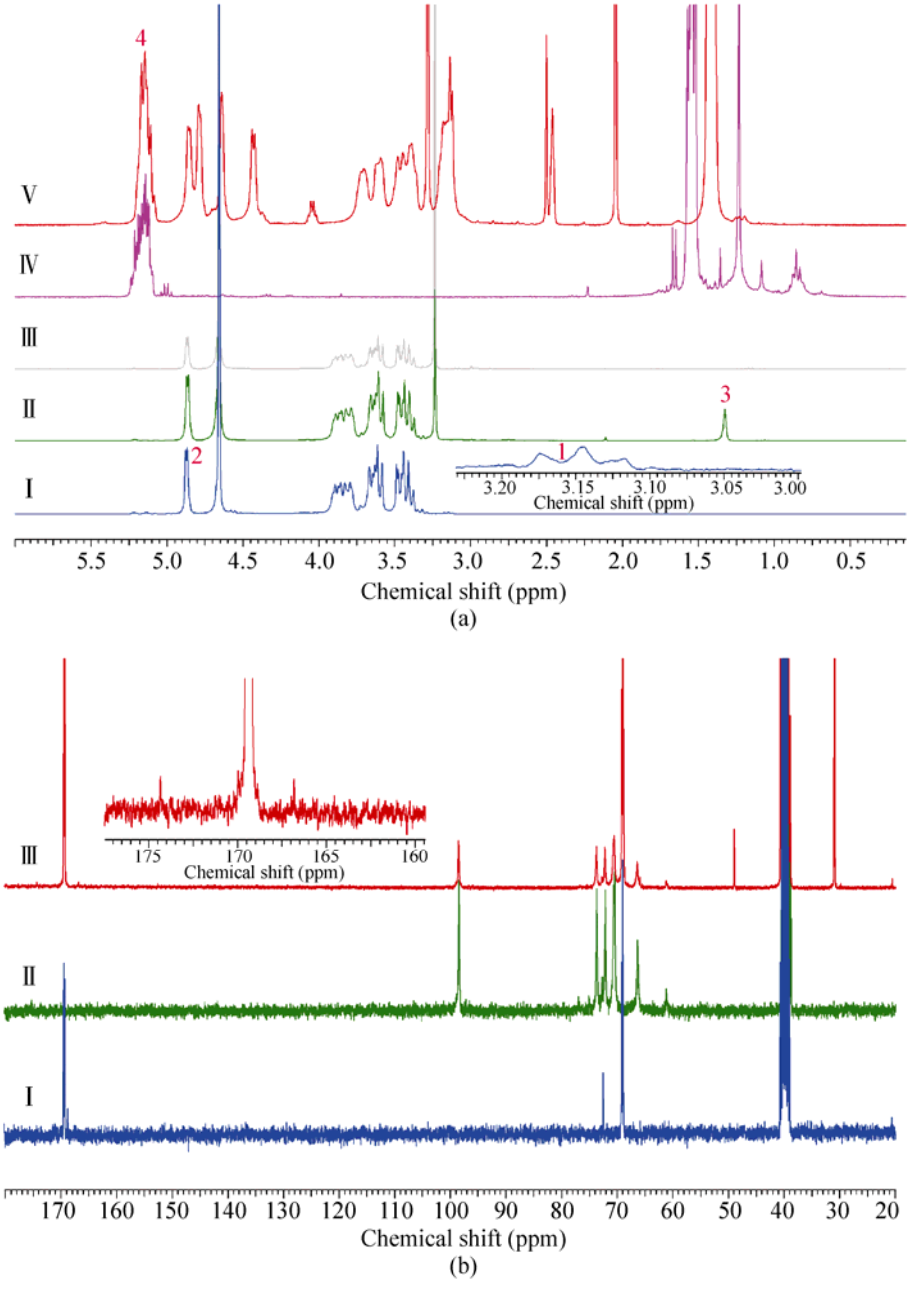

Figure 1 NMR spectra at various steps of the block copolymer synthesis: (a) proton NMR spectra of Ⅰ. Dextran 6 kDa (D_2O), Ⅱ. Dextran-NH-Et-NH-Boc (D_2O), Ⅲ. Dextran-NH-Et-NH_2 (D_2O), Ⅳ. PLA 20 kDa ($CDCl_3$), Ⅴ. Dextran-Et-PLA, or PLA20–Dex6 (DMSO-d_6); (b) ^{13}C NMR spectra of block copolymer Ⅰ. PLA 20 kDa, Ⅱ. Dextran 6 kDa, Ⅲ. Dex-Et-PLA (PLA20–Dex6) confirming the conjugation of dextran and PLA

PLA that is attached to the terminal amine of the ethylenediamine linker, while the peak at 169 ppm is assigned to the carbonyl carbon atom in the PLA backbone (Fig. 1(b)).

The size and morphology of NPs obtained using nine formulations of Dex-*b*-PLA block copolymers are shown in Fig. 2. Varying the M_W of PLA and dextran resulted in NPs with different sizes ranging from 15 to 70 nm. As shown in Fig. 2(a), increasing the M_W of PLA increased the particle size, whereas increasing the M_W of dextran decreased the particle size. The increase in size of NP cores formed by PLA with increasing M_W of the PLA chains has been demonstrated previously [22, 23], and it was confirmed here for the NPs composed of PLA with M_W of 10 kDa, 20 kDa, and 50 kDa. We postulate that the effect of the M_W of dextran on NP size is likely due to the configuration of dextran on the NP surface. Zahr et al. found that hydrophilic chains, such as PEG, with a M_W of 5 kDa or larger are able to "fold-down" onto the particle surface creating a mushroom conformation [24]. This phenomenon may explain why the NPs with longer dextran chains lead to smaller hydrodynamic diameters. The shorter dextran chain length has a smaller degree of freedom and is confined to a linear structure unlike those with longer chain length. The TEM image of NPs composed of PLA20–Dex6 (M_{WPLA} ~20 kDa, $M_{Wdextran}$ ~6 kDa) confirmed the particles exhibit a spherical structure (Fig. 2(b)).

Dex-*b*-PLA NPs with sizes under 50 nm were synthesized using a simple process of bulk nanoprecipitation. PLGA–PEG block copolymer was used as a commercial benchmark, which formed NPs with size 133.9 nm ± 6.1 nm following the same procedure. The particle size for PLGA–PEG is in agreement with previous literature values [25]. PLGA–PEG NPs with smaller particle sizes have been reported but their preparation required the assistance of microfluidic devices for enhanced control [17]. The particle size of Dex-*b*-PLA NPs, on the other hand, can be controlled simply by changing the M_W of the compositional polymers as exemplified in Fig. 2(a).

3.2 Doxorubicin encapsulation in Dex-*b*-PLA

Based on the size tuning as shown in Fig. 2, PLA20–Dex10 (M_{WPLA} ~20 kDa, $M_{Wdextran}$ ~10 kDa) and PLA20–Dex6 were selected for analyzing the encapsulation

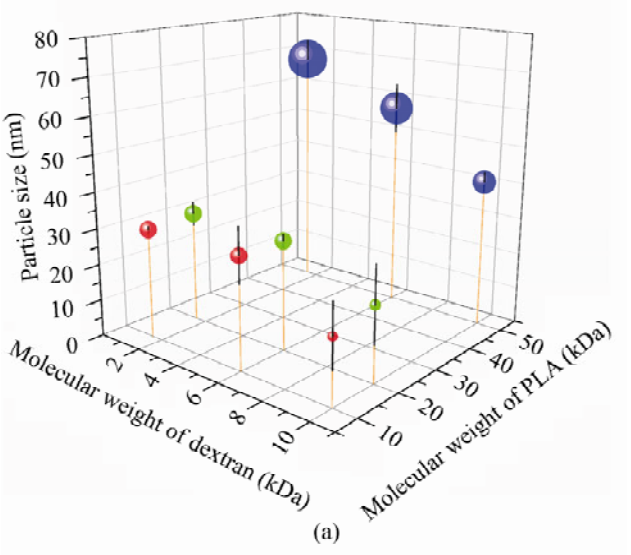

(a)

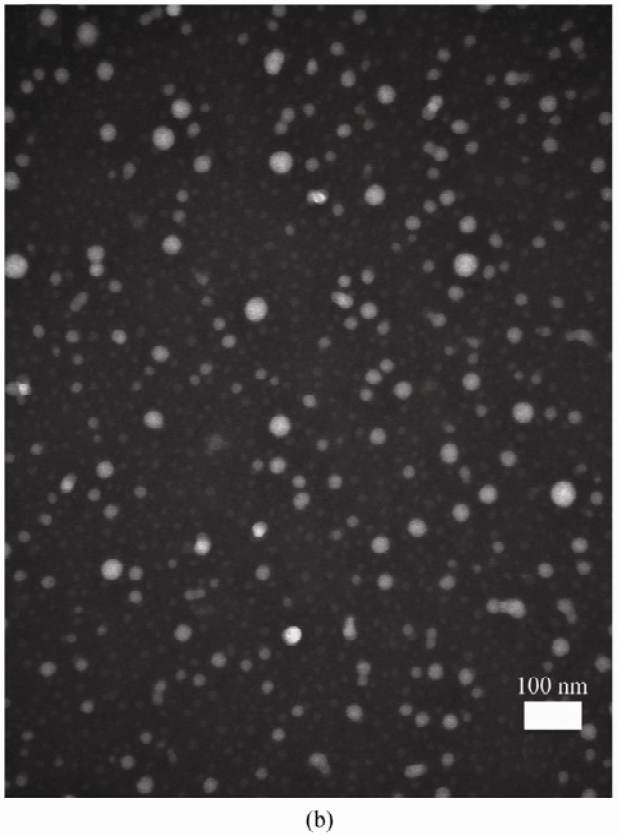

(b)

Figure 2 Particle size and morphology of Dex-*b*-PLA NPs: (a) effect of M_W of PLA and dextran on the sizes of the NPs formed from nine different polymers using PLA with M_W of 10 kDa (red), 20 kDa (green), and 50 kDa (blue), and dextran with M_W of 1.5 kDa, 6 kDa, and 10 kDa. The size of each data point represents the relative size of corresponding nanoparticles. The black bars represent the standard deviation of the particle sizes of each block copolymer; (b) TEM image of PLA20–Dex6 NPs (the scale bar is 100 nm) to demonstrate spherical shape of the nanoparticles

efficiencies and the drug loading using doxorubicin as a model hydrophobic drug (Fig. 3). The particle sizes for PLA20–Dex10 and PLA20–Dex6 were 20.5 nm and 30.1 nm respectively. Doxorubicin compounds were incorporated into NPs through a nanoprecipitation method. Both dextran-based NPs, PLA20–Dex10, and PLA20–Dex6 NPs, were found to encapsulate large amounts of doxorubicin with maximum loadings of 21.2 wt.%, and 10.5 wt.% respectively. The maximum loadings were achieved at 40 wt.% initial loading, and further increase in the initial loading did not increase the drug loading in the NPs due to aggregation of the particles. It is likely that PLA20–Dex10, with longer dextran chains than PLA20–Dex6, is likely to have more doxorubicin weakly associated on the NP surface or encapsulated near the surface of the NPs during nanoprecipitation. This effect was minimized by conducting ultrafiltration (MWCO = 10 kDa) after the nanoprecipitation, ensuring that the non-specifically bound drugs were removed from the NP suspension. The maximum drug loading in PLGA–PEG NPs, used as a control, was found to be 7.1 wt.%. It was found that excess initial loading caused more drug precipitation and particle aggregation during nanoprecipitation for PLGA–PEG NPs, whereas Dex-*b*-PLA NPs showed negligible size increases even at their maximum drug loading. The maximum doxorubicin loadings achieved with PLA20–Dex10 NPs were considerably higher than the most reported values using PEG-based NPs in the literature—which vary over 4.3%–11.2% for poly(*ε*-caprolactone)–PEG copolymers [26, 27], 8.7% for a poloxamer 407 and PEG hydrogel system [28], and 18% for PEG-poly(*β*-benzyl-*L*-aspartate)-based NPs [29]. The increased drug loading is most likely due to the greater hydrophilicity of dextran compared to PEG [30], which in turn reduces the probability of dextran chains from the block copolymers associating in the hydrophobic core of the NPs. The encapsulation efficiency and the total drug payload using the Dex-*b*-PLA system is comparable to commercially available liposomal systems such as the FDA approved Doxil®, which has a drug loading of 12.5% and DaunoXome®, which has a daunorubicin loading of 7.9% [31]. The concentration of doxorubicin in the Doxil® formulation translates into 6.25 mg/m^2 when Doxil® is administered at 50 mg/m^2 [31, 32]. The same physiological concentration of doxorubicin can theoretically be achieved using only 30 mg/m^2 of PLA20–Dex10 NP–doxorubicin formulation.

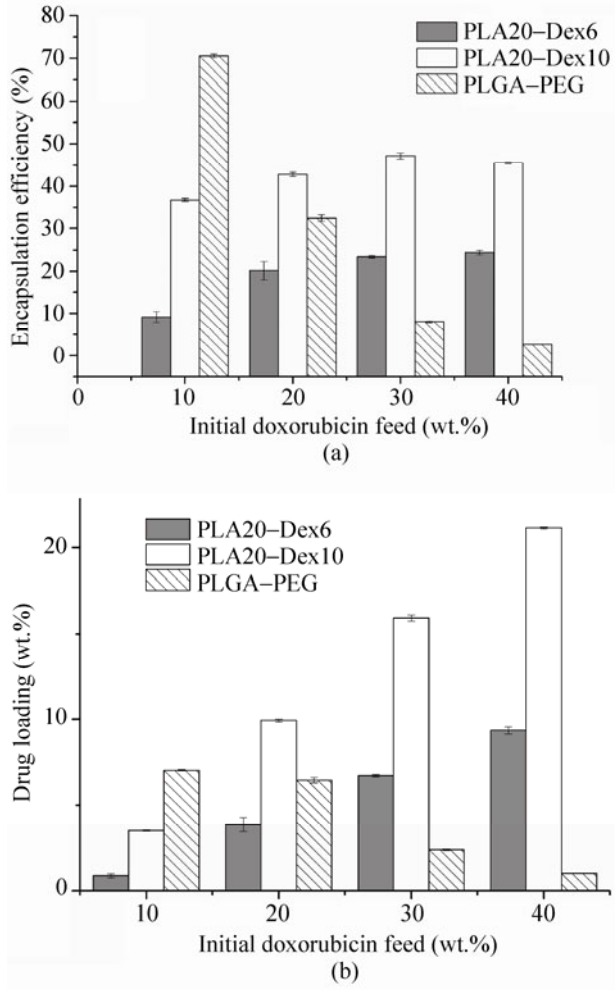

Figure 3 Drug encapsulation in NPs: (a) doxorubicin encapsulation efficiency in Dex-*b*-PLA and PLGA–PEG NPs using nanoprecipitation and (b) the corresponding drug loading wt.%. Solid gray columns are for PLA20–Dex6 NPs, solid white columns are for PLA20–Dex10 NPs, and columns with diagonal lines are for PLGA–PEG NPs (n = 3; mean ± S.D.)

3.3 Doxorubicin release profile from Dex-*b*-PLA

The *in vitro* release of doxorubicin from the NPs was carried out in pH 7.4 PBS buffer at 37 °C. As shown in Fig. 4, the release profile of doxorubicin from the NPs was characterized by an initial burst followed by a sustained-release phase. The burst-release region corresponds to drugs non-specifically bound on the surface of the NPs, or drugs encapsulated near the

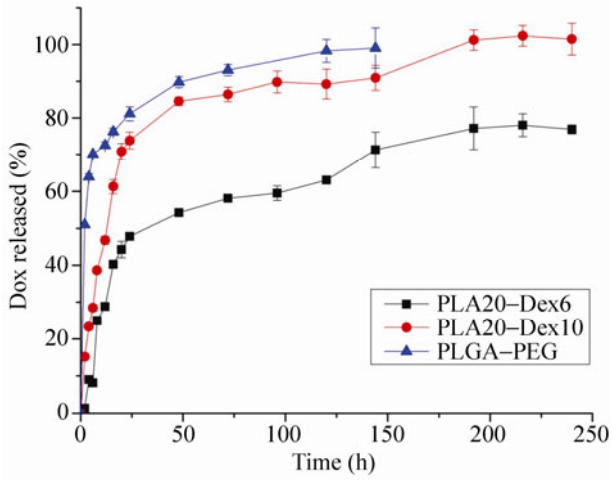

Figure 4 *In vitro* doxorubicin cumulative release profiles from Dex-*b*-PLA and PLGA–PEG NPs conducted in PBS at 37 ˚C. Solid squares (■) are for PLA20–Dex10, solid circles (●) are for PLA20–Dex6, and solid triangles (▲) are for PLGA–PEG NPs (n = 3; mean ± S.D.)

surface of the NPs during the nanoprecipitation procedure [33]. PLA20–Dex6 and PLA20–Dex10 NPs exhibited burst-release region within the initial 24 h, releasing up to 48% and 74% of the drug, respectively. The subsequent sustained-release phase of doxorubicin from PLA20–Dex6 and PLA20–Dex10 NPs continued for 192 h with similar rates of release from both NPs. The sustained-release phase most likely corresponds to the diffusional release of the drugs from the core of the NPs. In the control study using PLGA–PEG NPs, the burst-release phase of doxorubicin occurred within the first 6 h while the steady-release phase continued for up to 96 h, similar to what has been reported previously [34].

3.4 Hemolysis assay

Previous work has considered NPs with hemolysis ratios of less than 5% to be biocompatible [35]. It has been demonstrated that PLGA NPs stabilized by surfactants are severely hemolytic, with ratios of 80%, and hemolysis is reduced considerably by using a hydrophilic PEG surface in the case of PLGA–PEG NPs [36]. The same results are expected from the use of dextran-based NP formulation since dextran derivatives such as diethylaminoethyl-dextran have low (~5%) hemolysis ratios [37]. The block copolymer NPs formulated previously were tested for hemolytic activity at various concentrations (1–10 mg/mL). It was shown that all formulated NPs were not significantly hemolytic (< 5%) up to a concentration of 10 mg/mL in the blood (Fig. 5). The hemolysis by PLA20–Dex6 and PLA20–Dex 10 were similar since they have the same component polymers. For comparison, Doxil® (a liposomal formulation of doxorubicin) is usually administered at a dose of 50 mg/m^2 [32]. This dose translates to a concentration of 0.018 mg/mL in blood for an average human being (body surface area 1.79 m^2 [38], and blood volume 5 L) [39]. The tested hemocompatible concentration (10 mg/mL) for PLA–*b*–Dex NPs is considerably higher than the administered dose of Doxil®. Hence, PLA–*b*–Dex NPs promise a safe system for intravenous administration.

3.5 Pharmacokinetic and biodistribution of Dex-*b*-PLA NPs

The NP circulation half-life *in vivo* was characterized by measuring the amount of tritium [^{3}H]-PLA-radiolabeled nanocrystals that were incorporated in the NP formulations. Figure 6 shows the NP concentration in blood circulation at predetermined time intervals after intravenous administration. It is noted that the time-dependent NP concentration in the blood were characterized by two regions with distinct slopes.

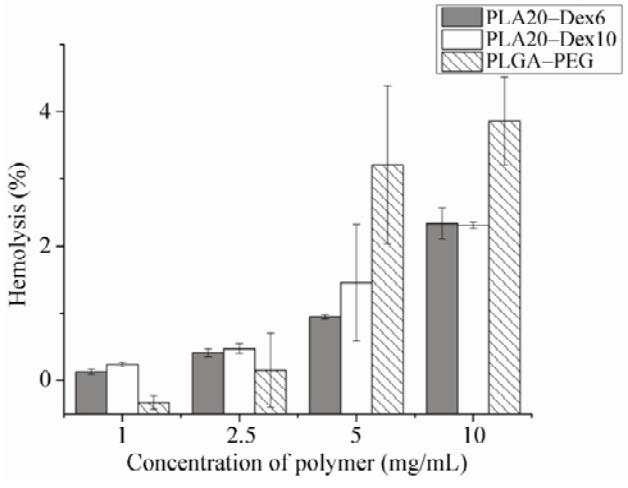

Figure 5 Hemolytic activity of Dex-*b*-PLA and PLGA–PEG NPs for concentrations relevant to the theoretical administered dose in blood. VBS was used as a negative control and deionized water was used as a positive control with sheep erythrocytes. Solid gray columns are for PLA20–Dex6 NPs, solid white columns are for PLA20–Dex10 NPs, and columns with diagonal lines are for PLGA–PEG NPs (n = 3; mean ± S.D.)

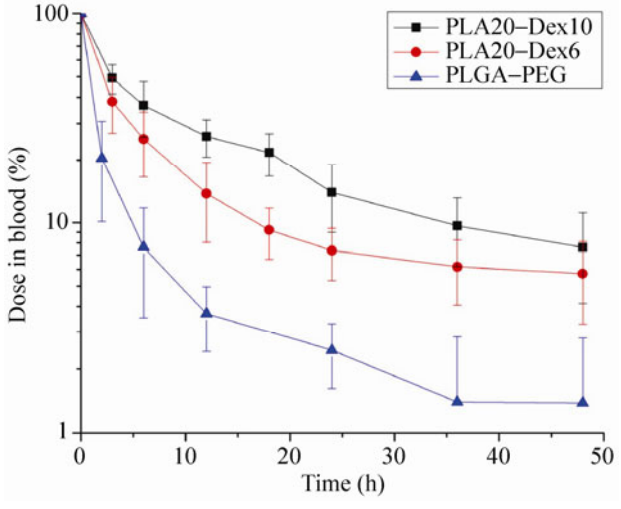

Figure 6 Pharmacokinetic profiles of Dex-*b*-PLA and PLGA–PEG NPs administered at 30 mg/kg i.v. to rats. The NP concentration in blood was tracked using [3H]-PLA-radiolabeled nanocrystals. Solid squares (■) are for PLA20–Dex10, solid circles (●) are for PLA20–Dex6, and solid triangles (▲) are for PLGA–PEG NPs (n = 5, mean ± S.D.)

The first region (the first ~18 h) corresponds to the initial clearance of the NPs from the blood circulation, whereas the second region indicates the terminal clearance of the NPs. The former region profiles the NP volume of distribution among vascular and extravascular tissues, while the terminal half-life relates to the systemic clearance phase of the NPs from the body [40]. The initial half-life ($t_{1/2}$), terminal half-life ($t_{z1/2}$), the blood retention time for 90% of the NPs ($t_{0.9}$), and area under curve (AUC) [41] of the three NPs are summarized in Table 1. At 24 h postinjection, rats were euthanized, and the major organs were harvested from the animals to evaluate the biodistribution of the NPs (Fig. 7). It was observed that all three NPs had maximum accumulation in the liver and the percentage distribution was similar for each type of NP. Higher accumulations in the spleen were observed with PLGA–PEG NPs compared to both Dex-*b*-PLA NPs ($p < 0.01$). Accumulation of NPs in all other organs was below 5% with similar amounts of accumulation for the different NPs in each organ.

Although all three types of NPs showed similar $t_{z1/2}$ values, both PLA20–Dex10 and PLA20–Dex6 NPs showed significantly higher values of $t_{1/2}$, $t_{0.9}$, and AUC compared to the corresponding values for the model NPs composed of PLGA–PEG. Previous studies

Table 1 Blood pharmacokinetic parameters for PLA20–Dex10, PLA20–Dex6, and PLGA–PEG NPs

	$t_{1/2}$ (h)	$t_{z1/2}$ (h)	$t_{0.9}$ (h)	AUC
PLA20–Dex10	12.3 ± 2.2	29.8 ± 1.0	38.3 ± 21.5	1040
PLA20–Dex6	7.2 ± 0.4	26.6 ± 3.1	17.9 ± 8.6	691
PLGA–PEG	3.7 ± 0.6	27.0 ± 2.3	5.0 ± 2.4	287

$t_{1/2}$: initial half-life; $t_{z1/2}$: terminal half-life; $t_{0.9}$: blood retention time for 90% of the NPs; AUC: area under curve.

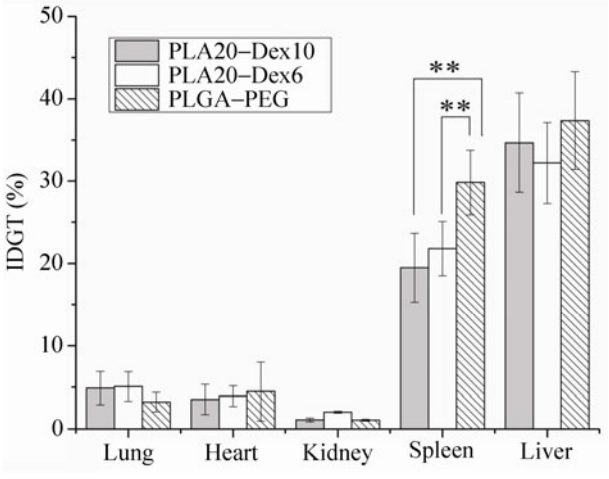

Figure 7 Biodistribution of Dex-*b*-PLA and PLGA–PEG NPs in various organs in rats at 24 h post-injection. Solid gray columns are for PLA20–Dex6 NPs, solid white columns are for PLA20–Dex10 NPs and columns with diagonal lines are for PLGA–PEG NPs (n = 5, mean ± S.D.). **: $p < 0.01$

mainly focused on $t_{z1/2}$ values for NPs but we have extracted $t_{0.9}$ values for comparison purposes. It was observed that $t_{0.9}$ values were only about 2 h for PEG-*b*-PLA NPs [41], 6 h for polyvinylpyrrolidone-based NPs [42], and about 8 h for chitosan-based NPs [43]. Not only do Dex-*b*-PLA NPs outperform these NPs with a $t_{0.9}$ of 38.3 h, they are also comparable to a 60 nm PEG-*b*-PCL system [44] and Stealth® liposomes [45], both of which have $t_{0.9}$ values over 48 h. In our study, the longer blood circulation times observed for Dex-*b*-PLA NPs, compared to PLGA–PEG NPs, is partially due to the size difference. A recent study by Rehor et al. showed that NPs with diameter of 40 nm had longer circulation half-life compared to larger NPs with diameter of 100 nm [46]. It is hypothesized that Dex-*b*-PLA NPs, having smaller sizes than PLGA–PEG NPs, have increased curvature that reduce protein adsorption, which may in turn result in slower

clearance rate by the RES. This is further supported by the longer blood circulation time of PLA20–Dex10 compared with PLA20–Dex6 since the former has a smaller particle size. In addition to their size effect on protein adsorption, it is also hypothesized that the abundant hydroxyl groups on the dextran surface may induce a sufficient hydration layer around the NPs to limit protein adsorption [47]. It has been reported that the accumulation rate in tissues such as the spleen increases with increase in the particle size [48], which is consistent with our findings. It has also been observed that the PEG coating in PEGylated particles can increase accumulation in the spleen [49], whereas the neutrality [50] and flexibility [51] of dextran chains on the NP surface can cause lower protein absorption leading to lower spleen accumulation. Dex-*b*-PLA NPs are expected to have low complement activation as observed for dextran-poly(methyl methacrylate) NPs, whose behaviour was similar to soluble dextran [51]. The lower accumulation of the Dex-*b*-PLA NPs in the spleen along with lower complement activation may contribute to their longer blood circulation [52]. The long circulation half-life of NP drug carriers is a crucial parameter in cancer therapy since it increases the probability of accumulating at cancerous tissues due to the EPR effect: particle sizes below 100 nm directly promote accumulation of NPs in the tumor sites, since the vascular pores around the tumor are at least 100 nm in size [15]. The size-tunable Dex-*b*-PLA system developed here presents a polymeric platform for systematically studying the effect of NP size on various *in vivo* characteristics such as biocompatibility, blood clearance, tumor accumulation, and biodistribution, allowing screening of candidates for further clinical evaluation.

4. Conclusion

A linear block copolymer of dextran and PLA has been synthesized and used for making size-tunable NPs. The size of NPs was controlled under 50 nm, simply by modulating the M_W of dextran and PLA. These NPs demonstrated efficient doxorubicin encapsulation, controlled drug release and hemocompatibility *in vitro* along with enhanced blood circulation half-life *in vivo*. These NPs provide promising tools for developing a controlled drug delivery system for nanomedicine applications.

Acknowledgements

This work was financially supported by Natural Sciences and Engineering Research Council of Canada.

References

[1] Jain, R. K.; Stylianopoulos, T. Delivering nanomedicine to solid tumors. *Nat. Rev. Clin. Oncol.* **2010**, *7*, 653–664.

[2] Gu, F. X.; Karnik, R.; Wang, A. Z.; Alexis, F.; Levy-Nissenbaum, E.; Hong, S.; Langer, R. S.; Farokhzad, O. C. Targeted nanoparticles for cancer therapy. *Nano Today* **2007**, *2*, 14–21.

[3] Pridgen, E. M.; Langer, R.; Farokhzad, O. C. Biodegradable, polymeric nanoparticle delivery systems for cancer therapy. *Nanomedicine* **2007**, *2*, 669–680.

[4] Kim, D. K.; Dobson, J. Nanomedicine for targeted drug delivery. *J. Mater. Chem.* **2009**, *19*, 6294–6307.

[5] Gref, R.; Minamitake, Y.; Peracchia, M. T.; Trubetskoy, V.; Torchilin, V.; Langer, R. Biodegradable long-circulating polymeric nanospheres. *Science* **1994**, *263*, 1600–1603.

[6] Gaucher, G.; Marchessault, R. H.; Leroux, J. Polyester-based micelles and nanoparticles for the parenteral delivery of taxanes. *J. Control. Release* **2010**, *143*, 2–12.

[7] Dong, Y.; Feng, S. *In vitro* and *in vivo* evaluation of methoxy polyethylene glycol–polylactide (MPEG–PLA) nanoparticles for small-molecule drug chemotherapy. *Biomaterials* **2007**, *28*, 4154–4160.

[8] Gursahani, H.; Riggs-Sauthier, J.; Pfeiffer, J.; Lechuga-Ballesteros, D.; Fishburn, C. S. Absorption of polyethylene glycol (PEG) polymers: The effect of PEG size on permeability. *J. Pharm. Sci.* **2009**, *98*, 2847–2856.

[9] Yang, J.; Cho, E.; Seo, S.; Lee, J.; Yoon, H.; Suh, J.; Huh, Y.; Haam, S. Enhancement of cellular binding efficiency and cytotoxicity using polyethylene glycol base triblock copolymeric nanoparticles for targeted drug delivery. *J. Biomed. Mater. Res. A* **2008**, *84A*, 273–280.

[10] Wei, X.; Gong, C.; Gou, M.; Fu, S.; Guo, Q.; Shi, S.; Luo, F.; Guo, G.; Qiu, L.; Qian, Z. Biodegradable poly(ε-caprolactone)–poly(ethylene glycol) copolymers as drug delivery system. *Int. J. Pharm.* **2009**, *381*, 1–18.

[11] Bazile, D.; Prudhomme, C.; Bassoullet, M. T.; Marlard, M.; Spenlehauer, G.; Veillard, M. Stealth Me.PEG–PLA nanoparticles avoid uptake by the mononuclear phagocytes system. *J. Pharm. Sci.* **1995**, *84*, 493–498.

[12] Lemarchand, C.; Gref, R.; Couvreur, P. Polysaccharide-decorated nanoparticles. *Eur. J. Pharm. Biopharm.* **2004**, *58*, 327–341.

[13] Kailasan, A.; Yuan, Q.; Yang, H. Synthesis and characterization of thermoresponsive polyamidoamine–polyethylene glycol–poly(*D*,*L*-lactide) core–shell nanoparticles. *Acta Biomater.* **2010**, *6*, 1131–1139.

[14] Owens, D. E.; Peppas, N. A. Opsonization, biodistribution, and pharmacokinetics of polymeric nanoparticles. *Int. J. Pharm.* **2006**, *307*, 93–102.

[15] Cho, K.; Wang, X.; Nie, S.; Chen, Z.; Shin, D. M. Therapeutic nanoparticles for drug delivery in cancer. *Clin. Cancer Res.* **2008**, *14*, 1310–1316.

[16] Jiang, W.; Kim, B. Y. S.; Rutka, J. T.; Chan, W. C. W. Nanoparticle-mediated cellular response is size-dependent. *Nat. Nanotechnol.* **2008**, *3*, 145–150.

[17] Karnik, R.; Gu, F.; Basto, P.; Cannizzaro, C.; Dean, L.; Kyei-Manu, W.; Langer, R.; Farokhzad, O. C. Microfluidic platform for controlled synthesis of polymeric nanoparticles. *Nano Lett.* **2008**, *8*, 2906–2912.

[18] Goodwin, A. P.; Tabakman, S. M.; Welsher, K.; Sherlock, S. P.; Prencipe, G.; Dai, H. Phospholipid–dextran with a single coupling point: A useful amphiphile for functionalization of nanomaterials. *J. Am. Chem. Soc.* **2009**, *131*, 289–296.

[19] Nouvel, C.; Frochot, C.; Sadtler, V.; Dubois, P.; Dellacherie, E.; Six, J. Polylactide-grafted dextrans: Synthesis and properties at interfaces and in solution. *Macromolecules* **2004**, *37*, 4981–4988.

[20] Chittasupho, C.; Xie, S.; Baoum, A.; Yakovleva, T.; Siahaan, T. J.; Berkland, C. J. ICAM-1 targeting of doxorubicin-loaded PLGA nanoparticles to lung epithelial cells. *Eur. J. Pharm. Sci.* **2009**, *37*, 141–150.

[21] Gu, F.; Zhang, L.; Teply, B. A.; Mann, N.; Wang, A.; Radovic-Moreno, A. F.; Langer, R.; Farokhzad, O. C. Precise engineering of targeted nanoparticles by using self-assembled biointegrated block copolymers. *Proc. Natl. Acad. Sci. U. S. A.* **2008**, *105*, 2586–2591.

[22] Riley, T.; Govender, T.; Stolnik, S.; Xiong, C. D.; Garnett, M. C.; Illum, L.; Davis, S. S. Colloidal stability and drug incorporation aspects of micellar-like PLA–PEG nanoparticles. *Colloids Surf. B-Biointerfaces.* **1999**, *19*, 147–159.

[23] Riley, T.; Stolnik, S.; Heald, C. R.; Xiong, C. D.; Garnett, M. C.; Illum, L.; Davis, S. S. ; Purkiss, S. C.; Barlow, R. J.; Gellert, P. R. Physicochemical evaluation of nanoparticles assembled from poly(lactic acid)–poly(ethylene glycol) (PLA–PEG) block copolymers as drug delivery vehicles. *Langmuir* **2001**, *17*, 3168–3174.

[24] Zahr, A. S.; Davis, C. A.; Pishko, M. V. Macrophage uptake of core–shell nanoparticles surface modified with poly(ethylene glycol). *Langmuir* **2006**, *22*, 8178–8185.

[25] Dhar, S.; Gu, F. X.; Langer, R.; Farokhzad, O. C.; Lippard, S. J. Targeted delivery of cisplatin to prostate cancer cells by aptamer functionalized Pt(IV) prodrug–PLGA–PEG nanoparticles. *Proc. Natl. Acad. Sci. U. S. A.* **2008**, *105*, 17356–17361.

[26] Shuai, X. T.; Ai, H.; Nasongkla, N.; Kim, S.; Gao, J. M. Micellar carriers based on block copolymers of poly(ε-caprolactone) and poly(ethylene glycol) for doxorubicin delivery. *J. Control. Release* **2004**, *98*, 415–426.

[27] He, Y. Y.; Zhang, Y.; Gu, C. H.; Dai, W. F.; Lang, M. D. Micellar carrier based on methoxy poly(ethylene glycol)–block–poly(epsilon-caprolactone) block copolymers bearing ketone groups on the polyester block for doxorubicin delivery. *J. Mater. Sci.-Mater. Med.* **2010**, *21*, 567–574.

[28] Missirlis, D.; Kawamura, R.; Tirelli, N.; Hubbell, J. A. Doxorubicin encapsulation and diffusional release from stable, polymeric, hydrogel nanoparticles. *Eur. J. Pharm. Sci.* **2006**, *29*, 120–129.

[29] Kataoka, K.; Harada, A.; Nagasaki, Y. Block copolymer micelles for drug delivery: Design, characterization and biological significance. *Adv. Drug Deliv. Rev.* **2001**, *47*, 113–131.

[30] Alpert, A. J. Hydrophilic-interaction chromatography for the separation of peptides, nucleic acids and other polar compounds. *J. Chromatogr. A* **1990**, *499*, 177–196.

[31] Drummond, D. C.; Meyer, O.; Hong, K.; Kirpotin, D. B.; Papahadjopoulos, D. Optimizing liposomes for delivery of chemotherapeutic agents to solid tumors. *Pharmacol. Rev.* **1999**, *51*, 691–744.

[32] Safra, T.; Muggia, F.; Jeffers, S.; Tsao-Wei, D. D.; Groshen, S.; Lyass, O.; Henderson, R.; Berry, G.; Gabizon, A. Pegylated liposomal doxorubicin (doxil): Reduced clinical cardiotoxicity in patients reaching or exceeding cumulative doses of 500 mg/m^2. *Ann. Oncol.* **2000**, *11*, 1029–1033.

[33] Magenheim, B.; Levy, M. Y.; Benita, S. A new *in vitro* technique for the evaluation of drugrelease profile from colloidal carriers–ultrafiltration technique at lowpressure. *Int. J. Pharm.* **1993**, *94*, 115–123.

[34] Esmaeili, F.; Ghahremani, M. H.; Ostad, S. N.; Atyabi, F.; Seyedabadi, M.; Malekshahi, M. R.; Amini, M.; Dinarvand, R. Folate-receptor-targeted delivery of docetaxel nanoparticles prepared by PLGA–PEG–folate conjugate. *J. Drug Target.* **2008**, *16*, 415–423.

[35] Dobrovoiskaia, M. A.; Clogston, J. D.; Neun, B. W.; Hall, J. B.; Patri, A. K.; McNeil, S. E. Method for analysis of nanoparticle hemolytic properties *in vitro*. *Nano Lett.* **2008**, *8*, 2180–2187.

[36] Kim, D.; El-Shall, H.; Dennis, D.; Morey, T. Interaction of PLGA nanoparticles with human blood constituents. *Colloid Surf. B-Biointerfaces* **2005**, *40*, 83–91.

[37] Fischer, D.; Li, Y. X.; Ahlemeyer, B.; Krieglstein, J.; Kissel, T. *In vitro* cytotoxicity testing of polycations: Influence of polymer structure on cell viability and hemolysis. *Biomaterials* **2003**, *24*, 1121–1131.

[38] Sacco, J. J.; Botten, J.; Macbeth, F.; Bagust, A.; Clark, P. The average body surface area of adult cancer patients in the UK: A multicentre retrospective study. *PLoS One* **2010**, *5*, e8933–e8933.

[39] Kusnierz-Glaz, C. R.; Still, B. J.; Amano, M.; Zukor, J. D.; Negrin, R. S.; Blume, K. G.; Strober, S. Granulocyte colony-stimulating factor-induced comobilization of $CD4^{-}CD8^{-}$ T cells and hematopoietic progenitor cells ($CD34^{+}$) in the blood of normal donors. *Blood* **1997**, *89*, 2586–2595.

[40] Yang, Z.; Leon, J.; Martin, M.; Harder, J. W.; Zhang, R.; Liang, D.; Lu, W.; Tian, M.; Gelovani, J. G.; Qiao, A. et al. Pharmacokinetics and biodistribution of near-infrared fluorescence polymeric nanoparticles. *Nanotechnology* **2009**, *20*, 165101.

[41] Gaucher, G.; Asahina, K.; Wang, J.; Leroux, J. Effect of poly(*N*-vinyl-pyrrolidone)-block-poly(*D*,*L*-lactide) as coating agent on the opsonization, phagocytosis, and pharmacokinetics of biodegradable nanoparticles. *Biomacromolecules* **2009**, *10*, 408–416.

[42] Gaur, U.; Sahoo, S. K.; De, T. K.; Ghosh, P. C.; Maitra, A.; Ghosh, P. K. Biodistribution of fluoresceinated dextran using novel nanoparticles evading reticuloendothelial system. *Int. J. Pharm.* **2000,** *202*, 1–10.

[43] He, C.; Hu, Y.; Yin, L.; Tang, C.; Yin, C. Effects of particle size and surface charge on cellular uptake and biodistribution of polymeric nanoparticles. *Biomaterials* **2010**, *31*, 3657–3666.

[44] Lee, H.; Fonge, H.; Hoang, B.; Reilly, R. M.; Allen, C. The effects of particle size and molecular targeting on the intratumoral and subcellular distribution of polymeric nanoparticles. *Mol. Pharm.* **2010**, *7*, 1195–1208.

[45] Allen, T. M.; Hansen, C. Pharmacokinetics of stealth versus conventional liposomes: effect of dose. *Biochim. Biophys. Acta-Biomembr.* **1991**, *1068*, 133–141.

[46] Rehor, A.; Schmoekel, H.; Tirelli, N.; Hubbell, J. A. Functionalization of polysulfide nanoparticles and their performance as circulating carriers. *Biomaterials* **2008**, *29*, 1958–1966.

[47] Portet, D.; Denizot, B.; Rump, E.; Hindre, F.; Le Jeune, J.; Jallet, P. Comparative biodistribution of thin-coated iron oxide nanoparticles TCION: Effect of different bisphosphonate coatings. *Drug Dev. Res.* **2001**, *54*, 173–181.

[48] Li, S.; Huang, L. Pharmacokinetics and biodistribution of nanoparticles. *Mol. Pharm.* **2008**, *5*, 496–504.

[49] Peracchia, M. T.; Fattal, E.; Desmaele, D.; Besnard, M.; Noel, J. P.; Gomis, J. M.; Appel, M.; d'Angelo, J.; Couvreur, P. Stealth® PEGylated polycyanoacrylate nanoparticles for intravenous administration and splenic targeting. *J. Control. Release* **1999**, *60*, 121–128.

[50] Chouly, C.; Pouliquen, D.; Lucet, I.; Jeune, J. J.; Jallet, P. Development of superparamagnetic nanoparticles for MRI: Effect of particle size, charge and surface nature on biodistribution. *J. Microencapsul.* **1996**, *13*, 245–255.

[51] Passirani, C.; Barratt, G.; Devissaguet, J.; Labarre, D. Long-circulating nanoparticles bearing heparin or dextran covalently bound to poly(methyl methacrylate). *Pharm. Res.* **1998**, *15*, 1046–1050.

[52] Meerasa, A.; Huang, J. G.; Gu, F. X. CH(50): A revisited hemolytic complement consumption assay for evaluation of nanoparticles and blood plasma protein interaction. *Curr. Drug Deliv.* **2011,** *8*, 290–298.